# Ubiquilin 2 modulates ALS/FTD-linked FUS–RNA complex dynamics and stress granule formation

Elizabeth J. Alexander[a,b], Amirhossein Ghanbari Niaki[c], Tao Zhang[a,b], Jaya Sarkar[c], Yang Liu[a,b], Raja Sekhar Nirujogi[d], Akhilesh Pandey[d,1], Sua Myong[c], and Jiou Wang[a,b,2]

[a]Department of Biochemistry and Molecular Biology, Johns Hopkins University Bloomberg School of Public Health, Baltimore, MD 21205; [b]Department of Neuroscience, Johns Hopkins University School of Medicine, Baltimore, MD 21205; [c]T. C. Jenkins Department of Biophysics, Johns Hopkins University, Baltimore, MD 21218; and [d]McKusick-Nathans Institute of Genetic Medicine, Johns Hopkins University School of Medicine, Baltimore, MD 21205

Edited by Clifford P. Brangwynne, Princeton University/Howard Hughes Medical Institute, Princeton, NJ, and accepted by Editorial Board Member Brenda A. Schulman October 18, 2018 (received for review July 12, 2018)

**The ubiquitin-like protein ubiquilin 2 (UBQLN2) has been genetically and pathologically linked to the neurodegenerative diseases amyotrophic lateral sclerosis (ALS) and frontotemporal dementia (FTD), but its normal cellular functions are not well understood. In a search for UBQLN2-interacting proteins, we found an enrichment of stress granule (SG) components, including ALS/FTD-linked heterogeneous ribonucleoprotein fused in sarcoma (FUS). Through the use of an optimized SG detection method, we observed UBQLN2 and its interactors at SGs. A low complexity, Sti1-like repeat region in UBQLN2 was sufficient for its localization to SGs. Functionally, UBQLN2 negatively regulated SG formation. UBQLN2 increased the dynamics of FUS–RNA interaction and promoted the fluidity of FUS–RNA complexes at a single-molecule level. This solubilizing effect corresponded to a dispersal of FUS liquid droplets in vitro and a suppression of FUS SG formation in cells. ALS-linked mutations in UBQLN2 reduced its association with FUS and impaired its function in regulating FUS–RNA complex dynamics and SG formation. These results reveal a previously unrecognized role for UBQLN2 in regulating the early stages of liquid–liquid phase separation by directly modulating the fluidity of protein–RNA complexes and the dynamics of SG formation.**

ALS | FTD | stress granule | ubiquilin 2 | FUS

Quality control and stress response programs are critical to cell survival. Defects in both protein quality control (PQC) and RNA homeostasis during stress are central to the pathogenesis of neurodegenerative diseases, such as amyotrophic lateral sclerosis (ALS) and frontotemporal dementia (FTD) (1). ALS, also known as Lou Gehrig's disease, is the most common adult-onset motor neuron disease, and is characterized by progressive loss of both upper and lower motor neurons, while FTD is the second most common type of dementia for people younger than 65 y of age, and is characterized by progressive changes in personality, behavior, and language ability (2, 3). The co-occurrence of ALS and FTD disease symptoms in up to 50% of cases suggests that ALS and FTD are part of a continuous clinical spectrum (ALS/FTD) (4). Increasing genetic and pathological evidence points to dysregulation of both protein and RNA homeostasis as two major processes underlying these diseases, but the interrelated functions of the molecular players are unclear (1).

The convergence of protein and RNA homeostasis in ALS/FTD pathogenesis suggests that common molecular players exist between the two pathways. ALS and FTD are genetically linked to both PQC factors in the proteasome and autophagy pathways, such as UBQLN2, SQSTM1, optineurin, and VCP, and to RNA binding proteins (RBPs), such as fused in sarcoma (FUS), TAR-DNA binding protein (TDP-43), Ewing sarcoma protein (EWS), TAT binding protein-associated factor 15 (TAF15), heterogeneous ribonucleoprotein A1 (hnRNPA1), and hnRNPA2/B1 (1). RBPs are a hallmark component of proteinaceous inclusions in patients who have ALS/FTD, suggesting that RBP solubility is compromised in patient cells. For example, the RBP FUS is common in inclusions in a large subset of patients with ALS/FTD (5). Over 40 mutations in FUS have been linked to ALS/FTD cases, including some of the most aggressive, juvenile-onset forms of the disease, in both familial and sporadic patients (6, 7). At the cellular level, FUS is involved in the maintenance of genomic integrity, transcription, pre-mRNA splicing, and microRNA regulation (8). It contains two amino-terminal intrinsically disordered regions that allow it to form biologically functional complexes in the cell, but also make it prone to aggregate. How FUS solubility is maintained in the cell and how FUS functions in ALS/FTD pathology are still unclear.

The formation of RNP granules by RBPs may be a critical aspect of PQC and RNA homeostasis in ALS/FTD disease pathogenesis (9, 10). Stress granules (SGs) are one type of RNP granule that forms during stress. Stresses such as heat and oxidative and osmotic stresses that trigger protein misfolding and stalled translation all induce the formation of SGs. Stalled translation initiation complexes, along with apoptotic factors, are sequestered in SGs until the stress subsides or the cell adapts to the conditions (11). Oligomerization of low-complexity, intrinsically disordered regions in RBPs bound to RNA drives SG

## Significance

**Amyotrophic lateral sclerosis (ALS) and frontotemporal dementia (FTD) are two devastating neurodegenerative diseases for which there are few treatments. ALS/FTD has been genetically and pathologically linked to both protein quality control (PQC) factors and RNA homeostasis, but the molecular players that bridge these pathways are not well characterized. Here, we identify a role for the ALS/FTD-linked PQC protein ubiquilin 2 (UBQLN2) in maintaining the solubility of RNA binding protein FUS in response to stress. UBQLN2 increases the dynamics of FUS–RNA complex formation, resulting in the negative regulation of stress granule (SG) formation. Because SGs potentially seed toxic inclusions of patients with ALS/FTD, these findings have implications for understanding ALS/FTD pathogenesis and designing new treatments for these diseases.**

Author contributions: E.J.A., J.S., S.M., and J.W. designed research; E.J.A., A.G.N., T.Z., J.S., and R.S.N. performed research; E.J.A., A.G.N., T.Z., J.S., Y.L., R.S.N., A.P., S.M., and J.W. analyzed data; and E.J.A., S.M., and J.W. wrote the paper.

The authors declare no conflict of interest.

This article is a PNAS Direct Submission. C.P.B. is a guest editor invited by the Editorial Board.



[1]Present addresses: Department of Laboratory Medicine and Pathology, Center for Individualized Medicine, Mayo Clinic, Rochester, MN 55905; and Manipal Academy of Higher Education, 576104 Manipal, Karnataka, India.

[2]To whom correspondence should be addressed. Email: jiouw@jhu.edu.

This article contains supporting information online at www.pnas.org/lookup/suppl/doi:10.1073/pnas.1811997115/-/DCSupplemental.

Published online November 15, 2018.

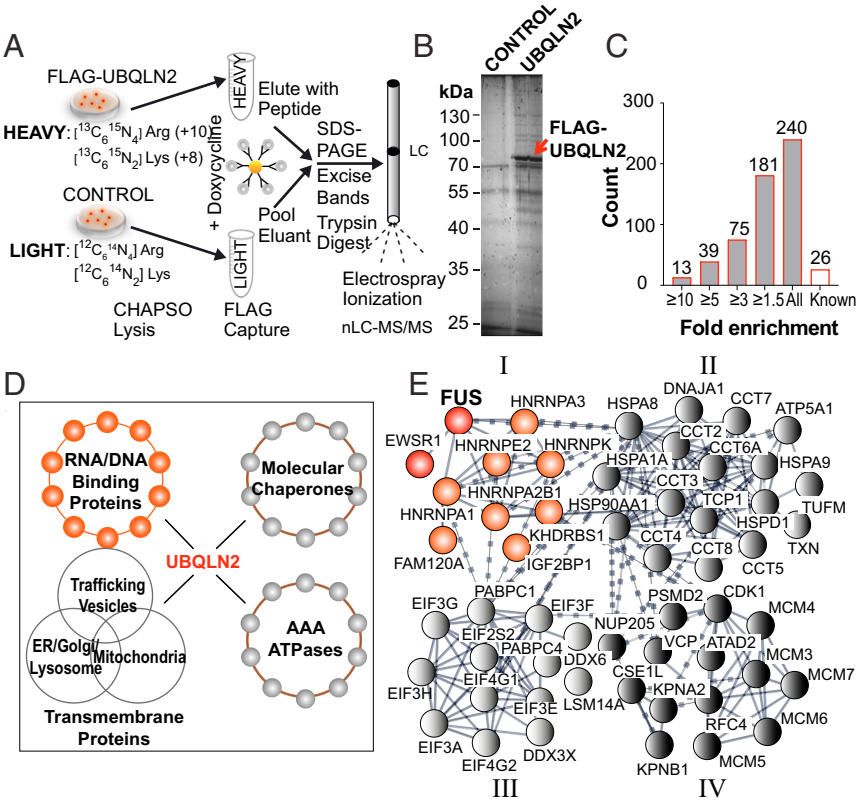


**Fig. 1.** SG components immunoprecipitate with UBQLN2. (*A*) Schematic of coimmunoprecipitation and SILAC nano-LC (nLC)-MS/MS analysis. Heavy-isotope-labeled stable HEK293T cell lines that inducibly express amino-terminal FLAG-UBQLN2 were treated with doxycycline and lysed in buffer containing the detergent CHAPSO. Light-isotope-labeled HEK293T cells treated with doxycycline were used as a control. Lysates were incubated with FLAG (M2) magnetic beads and eluted with FLAG peptide. Eluants were pooled at a 1:1 ratio and separated by SDS/PAGE. Bands were cut out, and proteins were digested with trypsin. Peptides were then extracted, separated via nLC, and injected via electrospray ionization into an LTQ Orbitrap Elite mass spectrometer for analysis. (*B*) Representative silver-stained gel of UBQLN2 CHAPSO immunoprecipitation. The red arrow points to exogenously expressed FLAG-UBQLN2 protein. (*C*) Cumulative frequency distribution of SILAC heavy (UBQLN2)/light (control) ratios from LC-MS/MS analysis of proteins that coimmunoprecipitated with FLAG-UBQLN2. A total of 240 putative interactors were identified, many of which cluster into SG component complexes shown in *E*. (*D*) Classes of UBQLN2 interactors grouped by domain structure. (*E*) STRING network of UBQLN2 interactors found in the G3BP-dependent SG proteome (56). Dotted and solid lines represent lower confidence and higher confidence connections, respectively. Members represented in the four clusters include hnRNPs (I), molecular chaperones (II), translation factors (III), and RNA trafficking proteins (IV). We focused further work on the class I hnRNP FUS.

formation in a process recently recognized as a liquid–liquid phase separation (LLPS) (12–15). This LLPS is tuned by both RNA length and structure. The dynamics of RBP-RNA binding determine RBP fate (16–18). Conversion of RBPs from a dynamic reversible liquid state into an irreversible solid state is proposed to be one of the early steps in disease pathogenesis associated with protein aggregation (9, 10). Importantly, the SG core components TIA-1, eIF3A, PABP, and eIF4G have been found in patient inclusions (10, 19). An increasing number of ALS/FTD-associated proteins found in patient inclusions have also been found in SGs, including FUS, TDP-43, C9orf72 protein and its polydipeptide repeats, ataxin 2, hnRNPA2/B1, hnRNPA1, SOD1, and profilin 1 (20–28). ALS/FTD-linked mutations in the RBPs FUS and hnRNPA1, which phase-separate into SGs, have also been shown to accelerate the phase transition of these proteins from a dynamic liquid state to a solid fibril state (14, 15, 27). PQC factors linked to ALS, such as VCP, play a role in both assembling and disassembling SGs and shuttling them to the autophagosome/lysosome system for degradation (29, 30). Other PQC factors implicated in SG formation include the Hsp70 heat shock protein and the deubiquitinase USP10 (31, 32). These PQC factors regulate SG protein turnover, but it is unclear how RBP-RNA dynamics are regulated to maintain RBP solubility during SG assembly.

In 2011, Deng et al. (33) identified single-point mutations in the *UBQLN2* gene that cause a rare X-linked form of ALS with dementia. UBQLN2 contains an amino-terminal ubiquitin-like (Ubl) domain and a carboxyl-terminal ubiquitin-associated (Uba) domain that allow it to both associate with the proteasome cap and bind polyubiquitinated chains (34–37). Based on this modular domain structure, it has been shown to act as a proteasome shuttle (38, 39), such as in directing misfolded mitochondrial precursor proteins, intermediate filament proteins, and endoplasmic reticulum-associated degradation (ERAD) substrates to the proteasome (40–42). Between the Ubl and Uba domains is a long linker region that contains a conserved set of Sti1-like repeats that interact with the ATPase domain of Hsp70 (43, 44). All of the ALS-linked mutations map to this linker region, but its function in concert with the Ubl and Uba domains is unclear. Ubiquilin 2 (UBQLN2) is one of four human paralogs, also including UBQLN1, UBQLN4, and UBQLN3, but only UBQLN2 contains a unique, mammalian-specific PXX repeat region (45). Mutations in this repeat reportedly inhibit proteasomal degradation (33, 46). Expression of mutant UBQLN2 in *Drosophila* and rodent models leads to cognitive deficits and motor neuron degeneration (43, 47–49), but its specific mechanism of action is not well understood.

Here, we report a direct role for UBQLN2 in modulating RNP solubility during SG formation. While searching for UBQLN2-interacting proteins through quantitative proteomics, we found an enrichment of SG components. In cells, UBQLN2 not only resides in SGs but also acts as a negative regulator of SG assembly. Mechanistically, UBQLN2 increased the fluidity of ALS-linked mutant FUS–RNA complexes, leading to an increase in the dispersion of FUS liquid droplets and suppression of FUS-seeded SGs. ALS-linked mutations impaired the function of UBQLN2 in regulating RNP dynamics and SG formation. Together, these results reveal a previously unrecognized role for UBQLN2 in directly modulating the early-stage dynamics of LLPS and SG formation associated with the RBP FUS.

## Results

**UBQLN2 Associates with SG Components.** To identify specific cellular functions for the UBQLN2 protein, we performed an unbiased quantitative proteomic screen for UBQLN2-interacting partners by stable isotope labeling with amino acids in cells (SILAC) coupled with nano-liquid chromatography tandem mass spectrometry (nLC-MS/MS) (50). Stable HEK293T cell lines with an integrated tetracycline-inducible FLAG-UBQLN2 construct were cultured with $^{13}C_6{}^{15}N_4$ Arg and $^{13}C_6{}^{15}N_2$ Lys heavy isotopes until complete labeling was attained. Proteins were extracted with

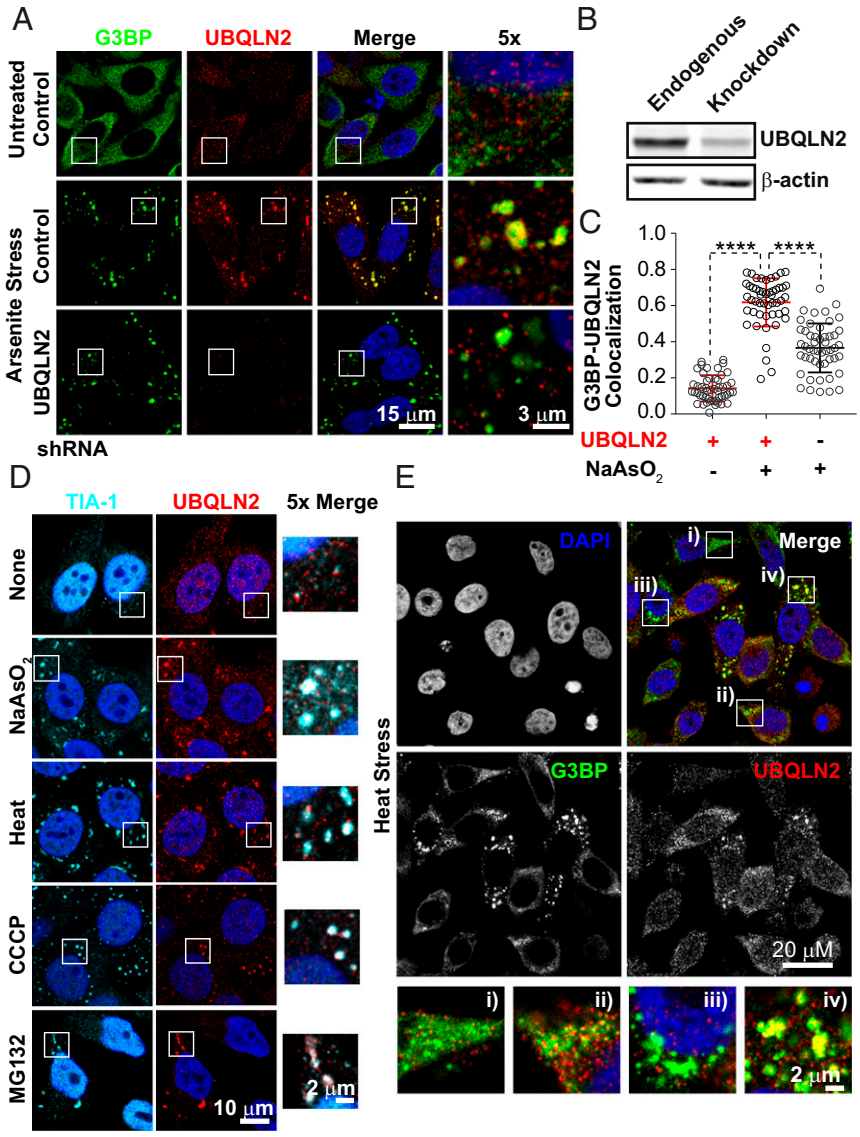


**Fig. 2.** UBQLN2 associates with SGs. (*A*) Immunofluorescence (IF) images of endogenous UBQLN2 at SGs in response to sodium arsenite stress (30 min, 0.5 mM $NaAsO_2$) in HeLa cells. G3BP marks SGs. Regions of UBQLN2-G3BP overlap appear yellow. Specific depletion of UBQLN2 eliminates the UBQLN2 signal and regions of overlap. Control shRNA is a scrambled nontargeting shRNA. (*B*) Western blot showing average endogenous UBQLN2 protein depletion 96 h after shRNA transfection. β-Actin is a loading control. (*C*) Scatter plot showing the Pearson's *R* coefficient of overlap between the G3BP (green) and UBQLN2 (red) signals shown in *A* for 50 individual cells (○) chosen at random. Error bars are SD. ****$P < 0.0001$ by Dunnett's multiple comparison test done with one-way ANOVA ($P < 0.0001$). UBQLN2 (–) represents the partial shRNA depletion of UBQLN2 shown in *B*. UBQLN2 appears to colocalize with SGs. (*D*) IF images of UBQLN2 localization under different stress conditions. HeLa cells were fixed and permeabilized simultaneously as shown in *A*. Stress conditions include: 0.5 h, 0.5 mM $NaAsO_2$; 1 h, 43.7 °C heat stress; 1.5 h, 1 μM CCCP in glucose-free media; 1 h, 10 μM MG132. (*E*) IF images showing localization of UBQLN2 to SGs with differing morphologies and localization after 30 min of heat stress at 43.7 °C. G3BP SG distribution is diffuse (*i*), concentrated but not punctate (*ii*), perinuclear punctate (*iii*), or large cytoplasmic punctate (*iv*).

CHAPSO lysis buffer, coimmunoprecipitated with FLAG-UBQLN2 on anti-FLAG (M2) beads, and eluted with FLAG peptide. Identically processed lysate from $^{12}C_6{}^{14}N_4$ Arg and $^{12}C_6{}^{14}N_2$ Lys light-labeled HEK293T cells treated with doxycycline was used as a control. Eluants were pooled and separated by SDS/PAGE, and peptides were digested and extracted for LC-MS/MS analysis (Fig. 1 *A* and *B*).

From this proteomic analysis, we identified 181 putative interactors for UBQLN2 enriched over 1.5-fold, 13 of which were enriched more than 10-fold (Fig. 1*C* and Dataset S1). These interactors could be subclassified by domain structure into four groups: molecular chaperones, AAA ATPases (ATPases associated with diverse cellular activities), RNA/DNA binding proteins, and transmembrane proteins (vesicle trafficking, ER/Golgi/lysosomal membrane, and mitochondrial membrane proteins) (Fig. 1*D*). Included in this list were previously identified UBQLN2 interactors: Hsp70 molecular chaperones HSPA1A, HSPA8, and HSPA13/Stch; ERAD chaperones FAF2/UBXD8 and HERPUD1; AAA ATPase VCP; proteasome cap subunits; RBPs hnRNPU and hnRNPA3; and membrane proteins ESyt2 and INSR (39, 42–44, 51–54) (Dataset S1). Western blot validation of some of the most enriched interactors confirmed our peptide search results from the LC-MS/MS analysis (*SI Appendix*, Fig. S1).

During the course of our analysis of UBQLN2 interactors, we noticed that members of every group except the membrane proteins were also represented in the SG proteome (55–58). To identify functional classes of proteins in SGs that UBQLN2 binds, we mapped the connectivity of SG-associated UBQLN2 interactors via STRING (Search Tool for the Retrieval of Interacting Genes/Proteins) network analysis (59). Four major classes of proteins emerged from this analysis: (*i*) hnRNPs, (*ii*) molecular chaperones, (*iii*) translation factors, and (*iv*) RNA trafficking proteins (Fig. 1*E*). The majority of ATP-dependent molecular chaperone assemblies found in the G3BP-dependent SG proteome (56), including VCP/p97, minichromosome maintenance protein complex (MCM), RuvB, and TriC (56), were represented in our SILAC analysis (groups II and IV). The karyopherins, A2 and B1, a class of proteins recently identified to solubilize hnRNP fibrils (60–63), were also represented in group IV. Notably, however, a subclass of ALS-linked hnRNPs known as the FET family, including FUS, EWS, and TAF15 (64–66), was also identified (group I). Among RBPs, FUS showed the highest peak intensity among the hnRNPs (Dataset S1). Overall, the results of this proteomic analysis indicated that UBQLN2 associates with SG components in the absence of stress.

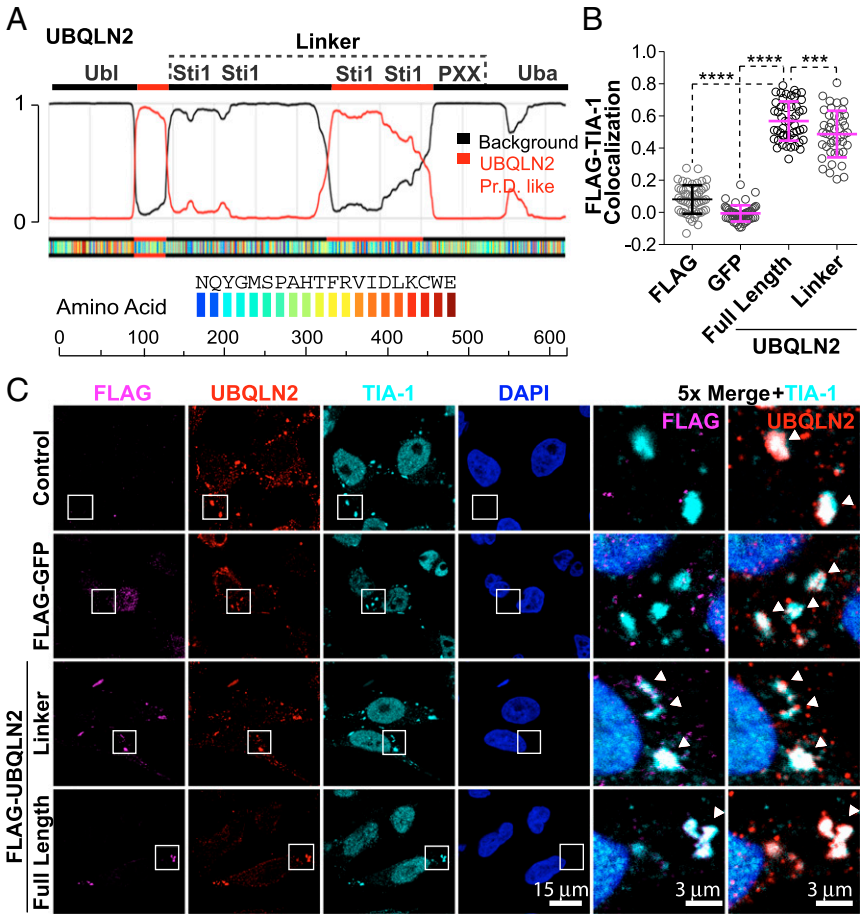


**Fig. 3.** Sti1-like linker alone is sufficient for UBQLN2 SG localization. (*A*) PrD analysis of UBQLN2. The dotted line highlights the bounds of the linker region tested in *B*. Identified PrD 1 is amino acids 105–143. PrD 2 is amino acids 338–460 of human UBQLN2. (*B*) Scatter plots showing the Pearson's *R* coefficient of overlap between FLAG-tagged proteins (magenta) with the SG marker TIA-1 (cyan) for 50 individual cells (○) chosen at random. FLAG-tagged proteins were expressed from an integrated short flippase recognition target (FRT) site in HeLa Flp-In TRex cells and exposed to 60 min of heat stress at 43.7 °C. Error bars are 1 SD from the mean. $^{****}P < 0.0001$, $^{***}P = 0.0006$; Dunnett's multiple comparison test. (*C*) Representative immunofluorescence images of HeLa Flp-In TRex cells expressing FLAG-tagged proteins as quantitated in *B*. The linker region alone drives UBQLN2 into SGs.

**UBQLN2 Associates with SGS.** To determine if UBQLN2 associates with SG components at SGs, we examined cells by immunofluorescence staining with UBQLN2-specific antibodies (*SI Appendix*, Fig. S2) under stress conditions. In response to acute sodium arsenite stress (0.5 mM for 30 min), endogenous UBQLN2 formed cytoplasmic puncta that colocalize with the core SG components G3BP and TIA-1 in HeLa cells (Fig. 2*A Middle* row and Fig. 2 *C* and *D*, second row). Depleting UBQLN2 with a specific shRNA (Fig. 2*B* and *SI Appendix*, Fig. S2) eliminated the UBQLN2 signal in G3BP-containing SGs, confirming that the UBQLN2 signal in SGs is specific (Fig. 2*A*, *Bottom* row and Fig. 2*C* and *SI Appendix*, Fig. S6, *Bottom* row).

Visualization of UBQLN2 in SGs was enhanced by use of an unconventional SG staining technique. We found that simultaneously fixing and permeabilizing cells with paraformaldehyde and Triton X-100 effectively limited the background cytoplasmic signal, revealing UBQLN2's underlying localization to SGs (*SI Appendix*, Fig. S3). UBQLN2 could also be detected in SGs by the conventional SG staining technique (11), but its localization with SG marker TIA-1 is largely obscured by its strong cytoplasmic signal (*SI Appendix*, Fig. S3, third row). This method of simultaneously fixing and permeabilizing cells was particularly effective in HeLa cells, where the cytoplasmic volume is more compressed than in other cell types, such as U2OS cells. We are not aware of any previously published reports in which this method was used systematically to detect SG components, but a similar approach was used previously to wash away nucleoplasmic components to enhance the detection of substructures in the nucleus (67, 68). Although this method does not allow calculation of the percentage of total protein in SGs, it does provide clear evidence of SG localization for proteins with strong cytoplasmic signals and did not appear to influence detection of the core SG components G3BP or TIA-1 used in later experiments. Using this method, we were able to show that other predicted SG components, such as VCP, TriC, Hsp72, and Hsc70 (56), are, in fact, present in SGs (*SI Appendix*, Fig. S4). As negative controls, the other functionally related Ubl/Uba proteins SQSTM1/p62 and BAG6 were not found to be components of SGs (*SI Appendix*, Fig. S5). Based on this finding, we believe this method may prove useful for examining the SG association of proteins with strong cytoplasmic signals.

P-bodies, unlike SGs, are constitutively present in the cytosol and contain enzymes for RNA decapping and degradation. Some components of P-bodies are also present in SGs, and vice versa (69). We next tested if UBQLN2 could also localize to P-bodies. Staining for UBQLN2, however, did not overlap with P-bodies under nonstress conditions (*SI Appendix*, Fig. S6). Only in cases where the P-bodies were directly juxtaposed to SGs did UBQLN2 show partial overlap with the P-body marker 4E-T (*SI Appendix*, Fig. S6, second row). Thus, UBQLN2 localizes to SGs, not P-bodies.

Since some proteins localize to SGs only under specific conditions (58, 69), we next tested if UBQLN2 localizes to SGs under other stress conditions. When treated with oxidative [carbonyl cyanide *m*-chlorophenyl hydrazone (CCCP) and $H_2O_2$], heat, proteotoxic (MG132), and osmotic (sorbitol and NaCl) stressors, UBQLN2 invariably localized to SGs (Fig. 2*D* and *SI Appendix*, Fig. S7). Some SG components are also dependent on cell line (58, 69), so we then tested if UBQLN2 localizes to SGs in other cell lines, such as HEK293T (human embryonic kidney), U2OS (bone marrow), and SHSY-5Y (neuroblastoma) cells. In all tested cell lines, UBQLN2 localized to SGs (*SI*

*Appendix*, Fig. S8). Based on these results, UBQLN2 appears to generally localize to SGs.

Notably, under all of the acute stress conditions tested initially, nearly all cells formed SGs containing UBQLN2, indicating that UBQLN2 is an SG component. However, SGs grow in size and change morphology and composition over time, so we then tested the types of granules with which UBQLN2 associates. After 30 min of heat stress, HeLa cells contained a variety of SG morphologies that we classified as (*i*) diffuse, (*ii*) concentrated but not punctate, (*iii*) perinuclear punctate, and (*iv*) cytoplasmic punctate (Fig. 2*E* and *SI Appendix*, Fig. S9*A*). Interestingly, enrichment of UBQLN2 was mainly found in large cytoplasmic punctate granules. UBQLN2 appeared to only weakly associate with perinuclear punctate SGs at 30 min (Fig. 2*E* and *SI Appendix*, Fig. S9*B*). These cells were rounded, and the cytoplasm was highly compressed. As stress was prolonged, this cell morphology predominated and UBQLN2 visibility in SGs weakened (*SI Appendix*, Fig. S9 *A* and *C*). This loss of UBQLN2 in SGs corresponded to the relocalization of UBQLN2 to the nucleus as previously reported (43). After this time point, cells began to undergo apoptosis. This selective association suggests that UBQLN2 localization to SGs is functionally linked to SG morphology and/or composition.

**The STI1 Linker Region Is Sufficient for UBQLN2 Sequestration into SGS.** To predict if annotated low-complexity regions in UBQLN2 might be functionally relevant to its localization to SGs, we first performed bioinformatic analysis of this region. Between the Ubl and Uba domains in UBQLN2 is a 474-aa stretch that composes the Sti1-like linker region. This region contains several low-complexity regions annotated by the SMART (Simple Modular Architecture Research Tool) algorithm (70). Analysis of the full-length protein via PLAAC (Prion-Like Amino Acid Composition) software revealed that UBQLN2 contains two putative prion-like domains (PrDs), a type of low-complexity domain that can mediate protein self-association (71), within this linker (Fig. 3*A*). The first region is located just downstream of the Ubl domain before the first set of Sti1-like repeats. The second region includes a second set of Sti1-like repeats specific to higher eukaryotes (44). This second region is the same one recently found to be essential for UBQLN2 oligomerization (72). The liquid droplet theory of SG formation predicts that low-complexity flexible regions in SG proteins can oligomerize to drive the phase separation of these proteins with RNA into granules. Based on this observation, we predicted that the Sti1-like linker would be sufficient to drive UBQLN2 into SGs.

To test if the Sti1-linker of UBQLN2 is sufficient to drive it into SGs, we constructed a new regulatable FLAG-UBQLN2 Flp-In HeLa cell line that would be ideal for imaging. This cell line inducibly expresses UBQLN2 at near-endogenous levels when treated with a low level of tetracycline (1 μg/mL). The full-length FLAG-UBQLN2, but not FLAG-GFP, colocalized with the SG marker TIA-1 after 30 min of heat stress, indicating that the FLAG tag itself does not drive protein localization to SGs. The expression of the FLAG-tagged Sti1-linker in the Flp-In system was relatively low, but it colocalized with SGs, indicating that the linker region is sufficient for UBQLN2 localization to SGs (Fig. 3 *B* and *C*).

**UBQLN2 Negatively Regulates SG Formation.** Overexpression of core SG components that contain low-complexity domains, such as TIA-1, G3BP, FUS and TDP-43, alone can drive SG formation (15, 22, 73–75). To test if UBQLN2 could seed SG formation, we overexpressed FLAG-tagged UBQLN2 in transiently transfected HeLa cells (Fig. 4*B*) and stained for the SG marker TIA-1. In no case did overexpressing UBQLN2 alone drive SG formation (Fig. 4 *A*, second column and *C*). Instead, overexpressing UBQLN2 had the effect of suppressing SG formation. The percentage of

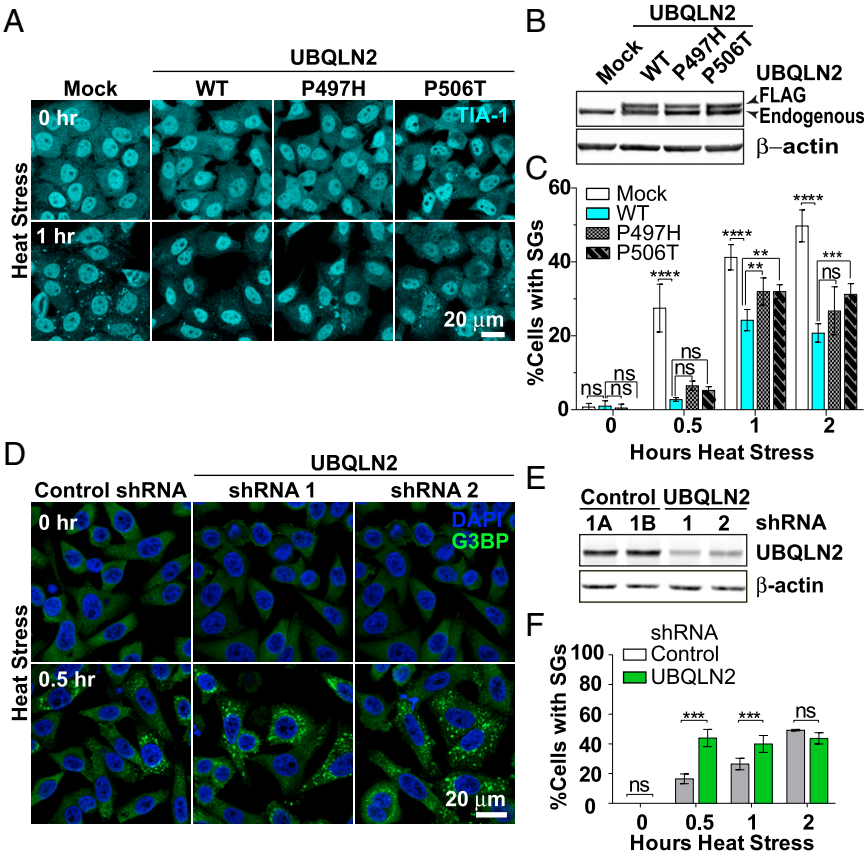


**Fig. 4.** UBQLN2 levels negatively regulate SG assembly. (*A*) Immunofluorescence (IF) maximum intensity projections (MIPs) of SGs in mock, FLAG-UBQLN2 wild-type (WT), FLAG-UBQLN2 P497H, and FLAG-UBQLN2 P506T transfected HeLa cells fixed and stained before and after heat stress. TIA-1 was used as an SG marker. (*B*) Western blot showing the level of UBQLN2 WT and mutant overexpression. β-Actin is used as a loading control. (*C*) Quantitation of percentage of cells with SGs larger than 1 μm shown in *A*. $****P < 0.0001$, $***P < 0.001$, $**P < 0.01$, $*P < 0.05$; Sidak's multiple comparison test. ns, not significant. (*D*) IF MIPs of SGs in control and UBQLN2-specific shRNA-treated HeLa cells before and after heat stress. G3BP was used as an SG marker, with DAPI marking the nuclei of individual cells. (*E*) Western blot showing the level of UBQLN2 depletion by the two UBQLN2-specific shRNAs. Approximately double the number of UBQLN2 shRNA-depleted cells show large cytoplasmic SGs after 30 min of heat stress. (*F*) Quantitation of percentage of cells with SG larger than 1 μm shown in *D*. $***P < 0.001$, Sidak's multiple comparison test. ns, not significant. A representative dataset is shown. More than 400 cells from four fields of view were imaged and averaged at each time point. Error bars are SD. The experiments were repeated using both G3BP and TIA-1 markers. UBQLN2 appears to negatively regulate SG formation in all cases.

CELL BIOLOGY

cells with large SGs was significantly decreased at all time points during heat stress in the presence of elevated levels of UBQLN2 (Fig. 4*C*). The ALS-linked mutant P497H or P506T partially interfered with UBQLN2's ability to suppress SG formation (Fig. 4 *A*, third and fourth columns and *C*) despite being overexpressed at the same level as the wild-type protein (Fig. 4*B*). This partial failure indicates that these missense mutations impair UBQLN2's function by disrupting large SG formation.

Next, we asked if depleting endogenous UBQLN2 would affect SG formation. Ninety-six hours after transfection with UBQLN2-specific shRNAs, HeLa cells were exposed to heat stress. The depletion of UBQLN2 resulted in a nearly twofold increase in the percentage of cells with large SGs, beginning at 30 min (Fig. 4 *D* and *F*). As the percentage of cells with SGs increased to nearly 100% at 2 h, UBQLN2 levels no longer affected the percentage of cells with large SGs, indicating that SGs enlarge faster when UBQLN2 levels are decreased (Fig. 4*F*). Even among the cells treated with UBQLN2 shRNA, those with higher levels of UBQLN2 expression showed a significantly lower level of large SGs (*SI Appendix*, Fig. S10), supporting this finding. This increase in the percentage of cells with large SGs corresponded to a significant increase in SG cross-sectional area and an increase in the number of all SGs per cell at time points before 2 h of heat stress (*SI Appendix*, Fig. S11). The change in the percentage of cells with large SGs upon UBQLN2 depletion could not be explained by an increase in the levels of the core stress component G3BP or TIA-1 protein (*SI Appendix*, Fig. S12), suggesting that depletion of UBQLN2 led to a concentration of SG components in larger SGs. Together, these data indicate that UBQLN2 negatively regulates SG size.

**UBQLN2 Forms a Complex with FUS and Suppresses Its Recruitment to SGs.** Based on the localization and negative regulatory function of UBQLN2 at SGs, we reasoned that UBQLN2 may physically interfere with the process of SG formation. To investigate UBQLN2's role in SG formation, we focused on its interaction with the highest ranked hnRNP in our SILAC analysis, FUS, which also has a well-established link to ALS pathology. FUS is an RBP that contains an amino-terminal, low-complexity, QGSY-rich, and Gly-rich region responsible for its oligomerization and phase separation into SGs. To confirm the interaction between UBQLN2 and FUS detected in our SILAC analysis (Fig. 1 and Dataset S1), we performed coimmunoprecipitation experiments with FLAG-tagged UBQLN2 and V5-tagged FUS. FUS immunoprecipitated with FLAG-tagged UBQLN2, but not with FLAG-tagged GUS control protein (Fig. 5*A*). The introduction of an ALS-linked UBQLN2 mutation, P497H or P506T, significantly decreased the interaction between UBQLN2 and FUS despite similar FUS protein expression level (Fig. 5 *A* and *B*).

We then tested if UBQLN2 regulates the recruitment of FUS to SGs. We first developed a system in HeLa cells to monitor SG formation with a FUS-GFP construct that spontaneously forms SGs in a small percentage of cells in the absence of stress. We designed this construct with a long C-terminal linker (13 aa) between FUS and GFP to limit GFP interference with the FUS QGSY-rich/Gly-rich intrinsically disordered region. UBQLN2 was cotransfected with FUS-GFP, and its effects on SG formation were monitored. Under heat stress, FUS-GFP–positive SGs robustly formed in cells with endogenous UBQLN2 levels (Fig. 5*C*). However, in cells in which UBQLN2 levels were elevated, there were significantly fewer large SGs present (Fig. 5 *C* and *D*), indicating that UBQLN2 interferes with FUS-GFP recruitment to SGs. These data are consistent with the observation that UBQLN2 negatively regulates SG formation.

Next, we asked if UBQLN2 affects the formation of FUS–RNA complexes in an electromobility shift assay (EMSA). Monomer FUS formed a discreet complex with polyuridine-50 ($pU_{50}$) RNA (Fig. 5*E*). Increasing the FUS protein concentration from 5 nM to 500 nM caused the probe signal to shift to a higher molecular weight position corresponding to FUS multimer. We then added native purified UBQLN2 protein to test the effect of UBQLN2 on FUS–RNA complex formation. At a 500 nM concentration of FUS, UBQLN2 supershifted the FUS–RNA complex. This result indicates that UBQLN2 can form a stable complex with FUS multimer in the presence of RNA. Furthermore, increasing concentrations of UBQLN2 protein freed RNA from the FUS–RNA monomer complex and RNA bound to FUS monomer from the FUS multimer complex (Fig. 5*E*). These data suggest that UBQLN2 can influence the formation of FUS–RNA complexes.

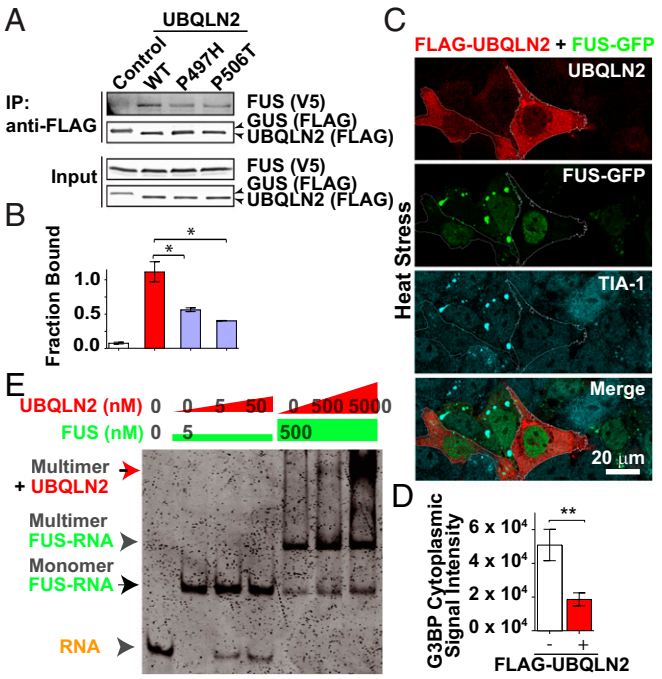


**Fig. 5.** UBQLN2 forms a complex with FUS and suppresses its SG formation. (*A*) FUS-V5 immunoprecipitates (IP) with FLAG-UBQLN2 in HEK293T cells. UBQLN2 ALS-linked missense mutations P497H and P506T partially disrupt UBQLN2's interaction with FUS. The FLAG-tagged plant reporter protein β-glucuronidase (GUS) was used as a control. (*B*) Quantitation of Western blot shown in *A*. The experiment was repeated twice, and the average results are presented here. Error bars are SD. $*P < 0.01$, Dunnett's multiple comparison test. (*C*) Immunofluorescence images of fixed HeLa cells cotransfected with FLAG-UBQLN2 and FUS-GFP. Cells overexpressing FLAG-UBQLN2 are outlined. TIA-1 marks SGs. (*D*) Quantitation of G3BP cytoplasmic signal in 13 pairs of cells expressing just FUS-GFP or FUS-GFP in the presence of FLAG-UBQLN2. $**P < 0.01$, two-tailed student's *t* test. UBQLN2 overexpression suppresses FUS-GFP SG formation in response to heat stress (30 min at 43.7 °C). (*E*) Coomassie blue-stained native PAGE gel of FUS-RNA and FUS-RNA-UBQLN2 by EMSA. The RNA probe is Cy3-labeled $pU_{40}$. Five nanomolar FUS results in a monomer FUS–RNA complex, whereas 500 nM FUS results in a shifted mobility multimer FUS–RNA complex. Addition of UBQLN2 to this preformed complex supershifts the multimer, but not the monomer, FUS–RNA complex.

**UBQLN2 Promotes ALS-Linked FUS–RNA Complex Dynamics.** Next, we asked if UBQLN2 could affect the dynamics of FUS–RNA complexes. Based on our observation that UBQLN2 freed RNA from the FUS–RNA monomer complex and FUS-RNA monomer from the FUS–RNA multimer complex, we expected that UBQLN2 would decrease the stability of FUS–RNA complexes formed. To test this hypothesis, we employed a single-molecule Förster resonance energy transfer (smFRET) assay to measure the dynamics of FUS–RNA complex assembly using a FUS mutant (R244C) with a nearly static interaction with RNA. The

conformation of a Cy3-Cy5–labeled RNA was measured by smFRET using a total internal reflection fluorescence (TIRF) microscope (100-ms resolution). Addition of RBP to the RNA changes the distance between the Cy3 and Cy5 tags reflected by the FRET ratio and alters the stability of the RNA conformation reflected by the FRET fluctuation. We expected that addition of UBQLN2 protein would increase the static interaction of $FUS^{R244C}$ with RNA (76). In the absence of the RBP FUS, the RNA probe exhibited a steady low FRET signal due to the Cy3-Cy5 dye separation by $pU_{50}$ (Fig. 6 *B* and *C*, panel 1). Addition of $FUS^{R244C}$ resulted in a nearly static Cy3-Cy5 FRET signal regardless of FUS mutant concentration. The addition of $FUS^{R244C}$ at a high concentration (1 μM) resulted in a highly static FUS–RNA interaction (Fig. 6 *B* and *C*, panel 3) in greater than 85% of molecules (Fig. 6*D*, 0 min). Addition of wild-type UBQLN2 to this complex consistently shifted its dynamics from static to dynamic. Within 5 min of UBQLN2 addition, the proportion of dynamic molecules increased from 18 to 55% (Fig. 6*D*). After 40 min, nearly 65% of molecules were classified as dynamic (Fig. 6*D*). However, not only did the number of dynamic molecules increase but also the frequency of the FRET fluctuation among those dynamic molecules. Analysis of 300 time intervals between FRET peaks from over 100 single molecules revealed that between 5 and 20 min, the time constant (τ) for the exponential decay fit decreased from ~10 s down to 1 s (Fig. 6*E*). This change in dynamics indicates that UBQLN2 is able to increase the dynamics of FUS mutant interaction with RNA over time.

The FUS-bound RNA FRET ratio reflecting the conformation of the complex was also altered by addition of UBQLN2. At a high FUS concentration (1 μM), two populations of high and intermediate FRET signal molecules exist. The intermediate FRET signal represents RNA bound to soluble multimerized FUS, whereas the high FRET signal represents RNA bound to higher order insoluble FUS. Addition of UBQLN2 to this complex led to a decrease in the intermediate FRET signal between 5 and 20 min (Fig. 6*C*, panels 3–6) on the same time scale that we saw an increase in FUS dynamics. As we observed for wild-type FUS (Fig. 5*E*), this shift indicates that UBQLN2 dissociates soluble FUS–RNA complexes. UBQLN2 was unable to alter the insoluble FUS–RNA complex composition. These data are consistent with the conclusion that UBQLN2 alters the dynamics of FUS–RNA complex formation. Furthermore, in contrast to wild-type UBQLN2, P497H and P506T mutant UBQLN2 failed to restore $FUS^{R244C}$ dynamics, with only 10% and 30% of molecules showing dynamic smFRET signals, respectively (Fig. 6 *B*, panels 7 and 8 and *D*). This failure to affect FUS–RNA complex assembly dynamics indicates a partial compromise of UBQLN2 function conferred by these ALS-linked mutations.

**UBQLN2 Supresses FUS-RNA LLPS.** The dynamics of RBP–RNA complex formation directly impact the LLPS of RBPs into liquid droplets (76). The dynamic interaction of wild-type FUS with RNA leads to the formation of smaller liquid droplets. In contrast, the static interaction of $FUS^{R244C}$ with RNA leads to the formation of large liquid droplets. Based on the finding that UBQLN2 increased FUS–RNA complex dynamics, we hypothesized that UBQLN2 addition would result in a decrease in FUS residence time in phase-separated droplets, and thus decrease the effective size of those droplets. To follow UBQLN2 activity, we performed a FUS liquid droplet assay by mixing $FUS^{R244C}$ protein with partially Cy3-labeled polyuridine 40 ($pU_{40}$) RNAs with or without UBQLN2. Tobacco etch virus (TEV) protease was added to cleave off the maltose-binding protein (MBP) solubility tag from FUS to trigger the formation of liquid droplets, and fluorescent images were taken at regular time intervals after protease digestion to monitor the size and number of the droplets. Within a period of 20 h, $FUS^{R244C}$-RNA droplets formed and increased in both size and number. When UBQLN2 was present, the $FUS^{R244C}$-RNA droplets formed were smaller in size but more numerous compared with those formed in the absence of UBQLN2 (Fig. 7 *A* and *B*, quantitated in Fig. 7 *C* and *D*). Notably, the $FUS^{R244C}$-RNA droplets in the absence of UBQLN2

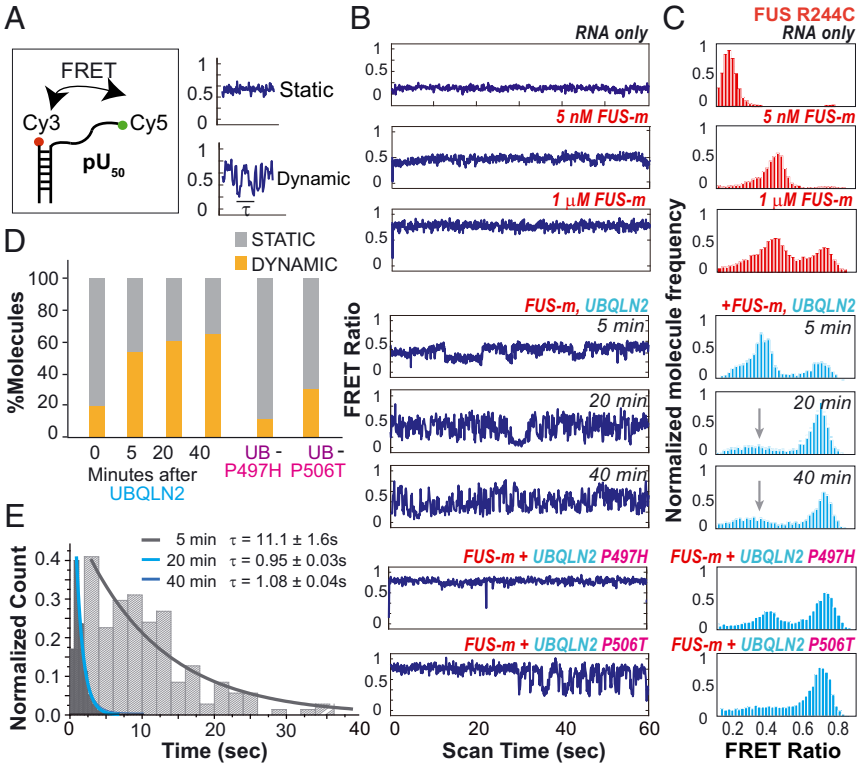


**Fig. 6.** UBQLN2 increases $FUS^{R244C}$–RNA interaction dynamics. (*A*) $pU_{50}$ probe design and sample static and dynamic single-molecule traces showing the dwell time constant (τ). (*B*) Representative traces showing the fluctuation of the FRET ratio for single molecules over time (panels 1–8). FUS-m, FUS mutant $FUS^{R244C}$. (*C*) Histograms of smFRET ratios for FUS-m mixed with $pU_{50}$ RNA (red; panels 1–3), FUS-m mixed with $pU_{50}$ in the presence of wild-type UBQLN2 (cyan; panels 4–6), and mutant UBQLN2 P497H and P506T (cyan; panels 7 and 8). The gray arrows point to the FRET peak broadened and flattened by UBQLN2 addition. (*D*) Percentage of single molecules with dynamic vs. static smFRET ratios. More than 1,000 traces were surveyed for this analysis. UBQLN2 mutant traces were collected between 20 and 40 min. Wild-type UBQLN2 addition alters $FUS^{R244C}$–RNA complex dynamics, while mutant UBQLN2 does so to a lesser extent. (*E*) τ of FRET fluctuation taken at 5, 20, and 40 min after addition of wild-type UBQLN2 to $FUS^{R244C}$. At 5–20 min after UBQLN2 addition, the FRET fluctuation rate dramatically increases for single molecules that are dynamic.

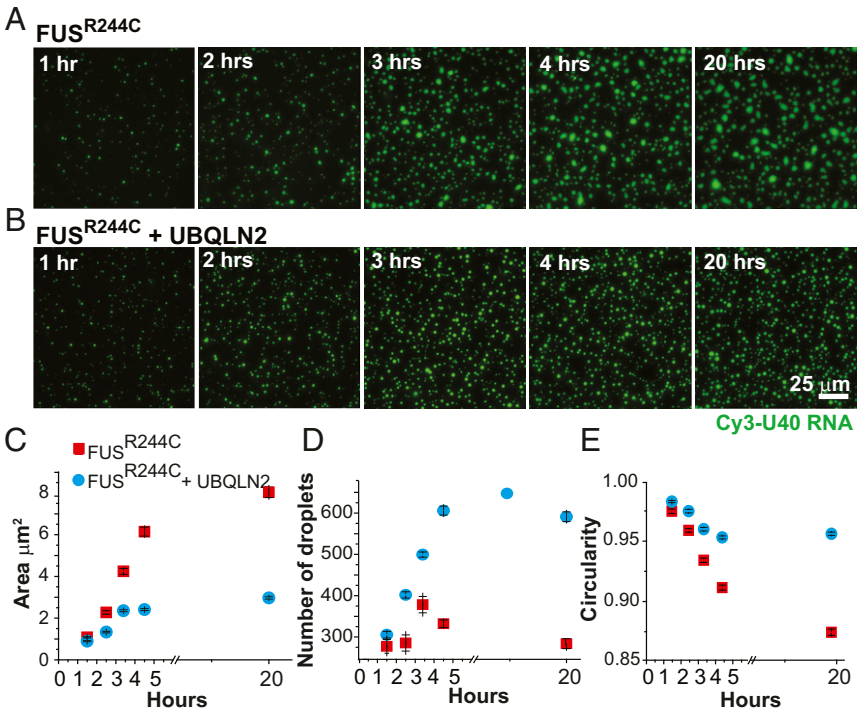


**Fig. 7.** UBQLN2 suppresses mutant FUS recruitment into phase-separated droplets. (*A*) Phase-separated droplets of FUS$^{R244C}$ mutants formed over 20 h. (*B*) Droplets of FUS$^{R244C}$ with UBQLN2 formed over 20 h. (*C*) Area of droplets taken over 20 h. Red and light blue indicate FUS$^{R244C}$ without and with UBQLN2 added, respectively. UBQLN2 addition leads to an increase in average liquid droplet area. (*D*) Number of droplets per imaging area. UBQLN2 addition leads to a decrease in liquid droplet number. (*E*) Circularity of droplets over 20 h. UBQLN2 addition leads to maintenance of liquid droplet circularity. More than 400 droplets in three to four fields of view were used for this analysis. All error bars shown are SEM. The experiment was repeated twice.

displayed nonspherical, irregular patterns, whereas those in the presence of UBQLN2 remained highly spherical over the entire time course. These nonspherical irregular droplets may represent the transition from the reversible liquid-like, phase-separated state of FUS to a more stable, solid state of FUS. Taken together, these results suggest that UBQLN2 is able to prevent the liquid-to-solid transition of FUS by increasing the FUS–RNA complex formation dynamics that underlie FUS phase separation. This activity is consistent with the negative regulatory role that UBQLN2 plays in SG formation.

## Discussion

In this study, we demonstrate a previously unknown role for UBQLN2 in regulating SG formation. UBQLN2 directly acts to promote the dynamics of FUS–RNA complexes and decrease the effective rate of FUS phase separation into liquid droplets, thereby suppressing SG formation. Mutations in UBQLN2 impair binding to FUS, resulting in loss of its ability to regulate the dynamics of FUS–RNA complexes and SG formation. These results expand the known functions of UBQLN2 and provide a direct link between protein and RNA homeostasis in normal stress responses and the pathogenesis of ALS/FTD.

These findings reveal a function of UBQLN2 independent of its previously established roles in mediating protein clearance. Instead of engaging with the protein degradation system via its Uba and Ubl domains, UBQLN2 associates with SG components through its Sti1-like linker region and influences the early process of molecular complex dynamics in phase separation that drives SG formation. Our quantitative proteomic analysis shows that UBQLN2 associates with SG components under homeostatic conditions, suggesting that these interactions exist before SG formation and UBQLN2 acts to regulate the exchange of these components into and out of SGs. Our time course analysis of SGs demonstrates that UBQLN2 is not a stable component of SGs but that its presence at the initial phases of SG assembly delays SG initiation, resulting in negative regulation of SG size. Notably, UBQLN2 does not appear to regulate the levels of core SG components but rather modulates the state of the components to be recruited. One of the main groups identified as UBQLN2-interacting SG components is the hnRNPs, consistent with previous reports that UBQLN2 interacts with hnRNPA1, hnRNPA3, and hnRNPU (52). We have focused on the hnRNP FUS, which contains a low-complexity region common among these hnRNPs, as a previously unknown interactor of UBQLN2 in our further analysis. This function is similar to the chaperone function of UBQLN2 in maintaining the solubility of transmembrane mitochondrial precursor proteins (40), but distinct in that it involves the modulation of protein–RNA interaction dynamics instead of its regulation of protein clearance.

We demonstrate that UBQLN2 has a direct function in promoting the dynamics of FUS–RNA complexes and suppressing the growth of FUS liquid droplets and their transition into more stable and solid states, which is consistent with the role of UBQLN2 in negatively regulating SG formation. This function is most reminiscent of the recently described role of ATP as a biological hydrotrope (77). Also, like the recently described nucleocytoplasmic transport protein transportin 1/karyopherin β2, UBQLN2 phase-separates itself, which has been attributed to the second set of Sti1-like repeats in UBQLN2 (72). Interestingly, UBQLN2 itself does not drive SG formation like other proteins with PrDs, but rather antagonizes the recruitment of SG components to SGs. These observations represent a potentially unrecognized mode of action for low-complexity domain proteins in SG formation. Previously described SG regulation has focused on regulation of levels of individual SG components, posttranslational modifications of SG components, and SG disaggregation through PQC mechanisms (29–32, 55, 56, 78, 79). Our proteomic analysis shows that UBQLN2 associates with many of the PQC factors, including ubiquitin, Hsp70, VCP, and TriC (Dataset S1), suggesting that UBQLN2 may cooperate with other PQC factors in SG regulation. However, in a mechanism that is not mutually exclusive, our present study demonstrates a distinct way that UBQLN2 directly regulates the dynamics of protein–RNA complexes in the early stages of SG formation (*SI Appendix*, Fig. S15). Although we chose to focus on FUS as a

previously characterized RBP recruited to SGs via its low-complexity domain and linked to ALS/FTD (15), we speculate that the solubility of other RBPs isolated in our proteomic screen that bind RNA and phase-separate into SGs could also be regulated by UBQLN2. Together, these findings expand our understanding of the different modes of SG regulation.

The results indicating that ALS/FTD-linked mutations in UBQLN2 (P497H and P506T) dampen UBQLN2's association with FUS, and thus impair the ability of UBQLN2 to regulate FUS–RNA interaction dynamics and SG formation, suggest that these processes may underlie the pathogenesis of ALS/FTD. FUS is one of a number of hnRNPs, including EWS, hnRNPA1, and hnRNPA2/B1, associated with ALS/FTD that we isolated in our proteomic screen that contain low-complexity flexible regions imparting the ability to phase-separate, but also to aggregate. Mutations in these hnRNPs have been reported to increase their propensity to collect in SGs, disrupting SG function as an adaptive stress response (13, 15, 27). Increased residence of hnRNPs in SGs may thus be directly linked to formation of abnormal SGs prone to form the pathological inclusions found in patients with ALS/FTD. We have shown that relative levels of UBQLN2 to SG components directly impact the rate of growth of large cytoplasmic SGs. Because ALS-linked mutations in UBQLN2 impair its interaction with hnRNPs or its function in maintaining hnRNP–RNA complex fluidity, the mutations could compromise the intrinsic ability of UBQLN2 to protect against aberrant SG formation and subsequent disease pathology.

This protective effect is consistent with previous reports that increasing the expression of UBQLN2 or its family members protects against the toxicity of a variety of neurodegeneration-related proteins, including amyloid-β, polyglutamine repeats, and TDP-43 (80–82). Collectively, the present study results reveal that UBQLN2 directly regulates the early stages of SG formation and suggest that it has a critical cytoprotective role at the junction between protein and RNA homeostasis, both of which underlie neurodegenerative diseases.

## Materials and Methods

**Antibodies for Western Blotting and Immunocytochemistry.** Rabbit anti-UBQLN2 (HPA0006431; Sigma) and mouse anti-UBQLN2 (NBP2; Novus) antibodies were used to specifically detect UBQLN2 via immunocytochemistry and Western blot (*SI Appendix*, Fig. S2). Goat anti–TIA-1 (C-20; Santa Cruz Biotechnology) and mouse anti-G3BP (611126; BD Biosciences) were used to detect SGs, and goat anti–4E-T (N-18; Santa Cruz Biotechnology) was used to detect P-bodies.

**Protein Purification.** His-GFP-TEV-UBQLN2 and His-FUS for the smFRET experiments were purified by nickel-nitrilotriacetic acid (NTA) affinity chromatography from *Escherichia coli*, followed by size exclusion chromatography (*SI Appendix*, Fig. S14). GST-FUS and GST-FUS$^{R244C}$ for the EMSA and MBP-TEV-FUS for the droplet assay were purified as described by Zhang et al. (83) and Burke et al. (84), respectively.

**Immunoprecipitation.** For the SILAC analysis, 3× FLAG-UBQLN2 was immunoprecipitated on FLAG beads and eluted with FLAG peptide in a 0.3% CHAPSO buffer [50 mM Hepes (pH 7.9), 150 mM NaCl, 2 mM EDTA]. SILAC LC-MS/MS analysis was performed as reported by Ong et al. (50). To validate the UBQLN2–FUS interaction, 3× FLAG-UBQLN2 and FUS-V5 were coimmunoprecipitated in 1% Nonidet P-40 and 0.05% deoxycholate buffer [50 mM Tris·HCl (pH 7.5), 150 mM NaCl, 0.4 mM EDTA] on protein A/G magnetic beads preequilibrated with anti-FLAG (M2) antibody (F3165; Sigma). Beads were washed five times with lysis buffer and bound protein was eluted with low pH buffer (21208; Pierce) into 1 M Tris (pH 8.0) buffer.

**EMSA.** Samples were prepared by mixing 0.5–1 nM Cy3-Cy5 dual-labeled RNA probe (used in smFRET experiments) with varying concentrations of proteins in binding buffer [50 mM Tris·HCl (pH 7.5), 150 mM KCl, 2 mM $MgCl_2$, 100 mM β-mercaptoethanol, 0.1 mg/mL BSA]. Samples were mixed with loading dye and run on a 6% DNA retardation polyacrylamide gel (Invitrogen). RNA mobility was visualized using a Typhoon scanner in fluorescent mode.

**smFRET via TIRF Microscopy.** Single-molecule imaging was performed as previously described by Zhang et al. (83).

**Liquid Droplet Assay.** One micromolar MBP-FUS, 1 μM unlabeled 40-nt-long $pU_{40}$, 4 μM UBQLN2, and 10 nM Cy3-labeled $pU_{40}$ were prepared in 50 mM Tris·HCl (pH 7.4), 100 mM NaCl, 1 mM EDTA, and 1 mM DTT buffer. TEV protease was added to cleave the MBP tag off of FUS. To visualize droplets, this mixture was added to the surface of an eight-well chambered cover glass (Nunc Lab-Tek) and imaged using a Nikon Ti Eclipse microscope equipped with a 100× oil-immersive objective, 555 nM laser, Cy3 emission filter, and EM CCD Andor camera in a 133-μm$^2$ field. We used intensity thresholding to mask and quantify the number and shape of the droplets in ImageJ (NIH).

**Statistical Analysis.** All graphs were prepared and data were analyzed in GraphPad Prism, except where noted. Column data were analyzed by a standard one-way ANOVA with Dunnett's method of correction for multiple paired comparisons. Grouped data were analyzed via a standard two-way ANOVA with Sidak's correction method for multiple comparisons.

Standard cell biology techniques for cell culture, transfection, immunoblotting, and SDS/PAGE separation and immunofluorescence microscopy were employed. Fixed cells were imaged on a Leica SP8 confocal microscope. Brightness and contrast adjustment, colocalization, SG size distribution, and percentage of cells with SGs analyses were performed in ImageJ. Prion-like amino acid analysis was performed using the Massachusetts Institute of Technology resource (plaac.wi.mit.edu/, accessed September 6, 2017).

**ACKNOWLEDGMENTS.** We thank Han-Xiang Deng for UBQLN2 cDNA with P497H and P506T mutations, Andrew Holland for the Flp-In HeLa cell line, Yihong Ye for the BAG6 antibody, and other J.W. laboratory members for helpful discussions. This work was supported by grants from the NIH (NS074324 and NS089616), Robert Packard Center for ALS Research at Johns Hopkins, Muscular Dystrophy Association, and ALS Association (to J.W.). E.J.A. was supported by an NIH Training Grant (T32CA009110).

1. Ling SC, Polymenidou M, Cleveland DW (2013) Converging mechanisms in ALS and FTD: Disrupted RNA and protein homeostasis. *Neuron* 79:416–438.
2. Ratnavalli E, Brayne C, Dawson K, Hodges JR (2002) The prevalence of frontotemporal dementia. *Neurology* 58:1615–1621.
3. van den Berg-Vos RM, et al. (2003) Sporadic lower motor neuron disease with adult onset: Classification of subtypes. *Brain* 126:1036–1047.
4. Van Langenhove T, van der Zee J, Van Broeckhoven C (2012) The molecular basis of the frontotemporal lobar degeneration-amyotrophic lateral sclerosis spectrum. *Ann Med* 44:817–828.
5. Mackenzie IR, Rademakers R, Neumann M (2010) TDP-43 and FUS in amyotrophic lateral sclerosis and frontotemporal dementia. *Lancet Neurol* 9:995–1007.
6. Kwiatkowski TJ, Jr, et al. (2009) Mutations in the FUS/TLS gene on chromosome 16 cause familial amyotrophic lateral sclerosis. *Science* 323:1205–1208.
7. Vance C, et al. (2009) Mutations in FUS, an RNA processing protein, cause familial amyotrophic lateral sclerosis type 6. *Science* 323:1208–1211.
8. Ishigaki S, Sobue G (2018) Importance of functional loss of FUS in FTLD/ALS. *Front Mol Biosci* 5:44.
9. Li YR, King OD, Shorter J, Gitler AD (2013) Stress granules as crucibles of ALS pathogenesis. *J Cell Biol* 201:361–372.
10. Aulas A, Vande Velde C (2015) Alterations in stress granule dynamics driven by TDP-43 and FUS: A link to pathological inclusions in ALS? *Front Cell Neurosci* 9:423.
11. Kedersha N, Anderson P (2007) Mammalian stress granules and processing bodies. *Methods Enzymol* 431:61–81.
12. Kroschwald S, et al. (2015) Promiscuous interactions and protein disaggregases determine the material state of stress-inducible RNP granules. *eLife* 4:e06807.
13. Lin Y, Protter DS, Rosen MK, Parker R (2015) Formation and maturation of phase-separated liquid droplets by RNA-binding proteins. *Mol Cell* 60:208–219.
14. Molliex A, et al. (2015) Phase separation by low complexity domains promotes stress granule assembly and drives pathological fibrillization. *Cell* 163:123–133.
15. Patel A, et al. (2015) A liquid-to-solid phase transition of the ALS protein FUS accelerated by disease mutation. *Cell* 162:1066–1077.
16. Elbaum-Garfinkle S, et al. (2015) The disordered P granule protein LAF-1 drives phase separation into droplets with tunable viscosity and dynamics. *Proc Natl Acad Sci USA* 112:7189–7194.
17. Langdon EM, et al. (2018) mRNA structure determines specificity of a polyQ-driven phase separation. *Science* 360:922–927.
18. Zhang H, et al. (2015) RNA controls PolyQ protein phase transitions. *Mol Cell* 60:220–230.
19. Mackenzie IR, et al. (2017) TIA1 mutations in amyotrophic lateral sclerosis and frontotemporal dementia promote phase separation and alter stress granule dynamics. *Neuron* 95:808–816.e9.

20. Bosco DA, et al. (2010) Mutant FUS proteins that cause amyotrophic lateral sclerosis incorporate into stress granules. *Hum Mol Genet* 19:4160–4175.
21. Sama RR, et al. (2013) FUS/TLS assembles into stress granules and is a prosurvival factor during hyperosmolar stress. *J Cell Physiol* 228:2222–2231.
22. Liu-Yesucevitz L, et al. (2010) Tar DNA binding protein-43 (TDP-43) associates with stress granules: Analysis of cultured cells and pathological brain tissue. *PLoS One* 5: e13250.
23. Dewey CM, et al. (2011) TDP-43 is directed to stress granules by sorbitol, a novel physiological osmotic and oxidative stressor. *Mol Cell Biol* 31:1098–1108.
24. Boeynaems S, et al. (2017) Phase separation of C9orf72 dipeptide repeats perturbs stress granule dynamics. *Mol Cell* 65:1044–1055.e5.
25. Nonhoff U, et al. (2007) Ataxin-2 interacts with the DEAD/H-box RNA helicase DDX6 and interferes with P-bodies and stress granules. *Mol Biol Cell* 18:1385–1396.
26. Figley MD, Bieri G, Kolaitis RM, Taylor JP, Gitler AD (2014) Profilin 1 associates with stress granules and ALS-linked mutations alter stress granule dynamics. *J Neurosci* 34: 8083–8097.
27. Kim HJ, et al. (2013) Mutations in prion-like domains in hnRNPA2B1 and hnRNPA1 cause multisystem proteinopathy and ALS. *Nature* 495:467–473.
28. Gal J, et al. (2016) ALS mutant SOD1 interacts with G3BP1 and affects stress granule dynamics. *Acta Neuropathol* 132:563–576.
29. Buchan JR, Kolaitis RM, Taylor JP, Parker R (2013) Eukaryotic stress granules are cleared by autophagy and Cdc48/VCP function. *Cell* 153:1461–1474.
30. Seguin SJ, et al. (2014) Inhibition of autophagy, lysosome and VCP function impairs stress granule assembly. *Cell Death Differ* 21:1838–1851.
31. Ganassi M, et al. (2016) A surveillance function of the HSPB8-BAG3-HSP70 chaperone complex ensures stress granule integrity and dynamism. *Mol Cell* 63:796–810.
32. Kedersha N, et al. (2016) G3BP-Caprin1-USP10 complexes mediate stress granule condensation and associate with 40S subunits. *J Cell Biol* 212:845–860.
33. Deng HX, et al. (2011) Mutations in UBQLN2 cause dominant X-linked juvenile and adult-onset ALS and ALS/dementia. *Nature* 477:211–215.
34. Kleijnen MF, Alarcon RM, Howley PM (2003) The ubiquitin-associated domain of hPLIC-2 interacts with the proteasome. *Mol Biol Cell* 14:3868–3875.
35. Ko HS, Uehara T, Tsuruma K, Nomura Y (2004) Ubiquilin interacts with ubiquitylated proteins and proteasome through its ubiquitin-associated and ubiquitin-like domains. *FEBS Lett* 566:110–114.
36. Walters KJ, Kleijnen MF, Goh AM, Wagner G, Howley PM (2002) Structural studies of the interaction between ubiquitin family proteins and proteasome subunit S5a. *Biochemistry* 41:1767–1777.
37. Raasi S, Varadan R, Fushman D, Pickart CM (2005) Diverse polyubiquitin interaction properties of ubiquitin-associated domains. *Nat Struct Mol Biol* 12:708–714.
38. Gao L, et al. (2003) Interaction with a ubiquitin-like protein enhances the ubiquitination and degradation of hepatitis C virus RNA-dependent RNA polymerase. *J Virol* 77:4149–4159.
39. Kleijnen MF, et al. (2000) The hPLIC proteins may provide a link between the ubiquitination machinery and the proteasome. *Mol Cell* 6:409–419.
40. Itakura E, et al. (2016) Ubiquilins chaperone and triage mitochondrial membrane proteins for degradation. *Mol Cell* 63:21–33.
41. Gavriilidis C, et al. (2018) The MTM1-UBQLN2-HSP complex mediates degradation of misfolded intermediate filaments in skeletal muscle. *Nat Cell Biol* 20:198–210.
42. Xia Y, et al. (2014) Pathogenic mutation of UBQLN2 impairs its interaction with UBXD8 and disrupts endoplasmic reticulum-associated protein degradation. *J Neurochem* 129:99–106.
43. Hjerpe R, et al. (2016) UBQLN2 mediates autophagy-independent protein aggregate clearance by the proteasome. *Cell* 166:935–949.
44. Kaye FJ, et al. (2000) A family of ubiquitin-like proteins binds the ATPase domain of Hsp70-like Stch. *FEBS Lett* 467:348–355.
45. Marín I (2014) The ubiquilin gene family: Evolutionary patterns and functional insights. *BMC Evol Biol* 14:63.
46. Chang L, Monteiro MJ (2015) Defective proteasome delivery of polyubiquitinated proteins by ubiquilin-2 proteins containing ALS mutations. *PLoS One* 10:e0130162.
47. Wu Q, et al. (2015) Pathogenic Ubqln2 gains toxic properties to induce neuron death. *Acta Neuropathol* 129:417–428.
48. Kim SH, et al. (2018) Mutation-dependent aggregation and toxicity in a Drosophila model for UBQLN2-associated ALS. *Hum Mol Genet* 27:322–337.
49. Le NT, et al. (2016) Motor neuron disease, TDP-43 pathology, and memory deficits in mice expressing ALS-FTD-linked UBQLN2 mutations. *Proc Natl Acad Sci USA* 113: E7580–E7589.
50. Ong SE, et al. (2002) Stable isotope labeling by amino acids in cell culture, SILAC, as a simple and accurate approach to expression proteomics. *Mol Cell Proteomics* 1: 376–386.
51. Kim TY, Kim E, Yoon SK, Yoon JB (2008) Herp enhances ER-associated protein degradation by recruiting ubiquilins. *Biochem Biophys Res Commun* 369:741–746.
52. Gilpin KM, Chang L, Monteiro MJ (2015) ALS-linked mutations in ubiquilin-2 or hnRNPA1 reduce interaction between ubiquilin-2 and hnRNPA1. *Hum Mol Genet* 24: 2565–2577.
53. Kurlawala Z, Shah PP, Shah C, Beverly LJ (2017) The STI and UBA domains of UBQLN1 are critical determinants of substrate interaction and proteostasis. *J Cell Biochem* 118:2261–2270.
54. Kurlawala Z, et al. (2017) Regulation of insulin-like growth factor receptors by Ubiquilin1. *Biochem J* 474:4105–4118.
55. Ohn T, Kedersha N, Hickman T, Tisdale S, Anderson P (2008) A functional RNAi screen links O-GlcNAc modification of ribosomal proteins to stress granule and processing body assembly. *Nat Cell Biol* 10:1224–1231.
56. Jain S, et al. (2016) Atpase-modulated stress granules contain a diverse proteome and substructure. *Cell* 164:487–498.
57. Youn JY, et al. (2018) High-density proximity mapping reveals the subcellular organization of mRNA-associated granules and bodies. *Mol Cell* 69:517–532.e11.
58. Markmiller S, et al. (2018) Context-dependent and disease-specific diversity in protein interactions within stress granules. *Cell* 172:590–604.e13.
59. Szklarczyk D, et al. (2015) STRING v10: Protein-protein interaction networks, integrated over the tree of life. *Nucleic Acids Res* 43:D447–D452.
60. Guo L, et al. (2018) Nuclear-import receptors reverse aberrant phase transitions of RNA-binding proteins with prion-like domains. *Cell* 173:677–692 e620.
61. Qamar S, et al. (2018) FUS phase separation is modulated by a molecular chaperone and methylation of arginine cation-$\pi$ interactions. *Cell* 173:720–734.e15.
62. Hofweber M, et al. (2018) Phase separation of FUS is suppressed by its nuclear import receptor and arginine methylation. *Cell* 173:706–719.e13.
63. Yoshizawa T, et al. (2018) Nuclear import receptor inhibits phase separation of FUS through binding to multiple sites. *Cell* 173:693–705.e22.
64. Couthouis J, et al. (2012) Evaluating the role of the FUS/TLS-related gene EWSR1 in amyotrophic lateral sclerosis. *Hum Mol Genet* 21:2899–2911.
65. Couthouis J, et al. (2011) A yeast functional screen predicts new candidate ALS disease genes. *Proc Natl Acad Sci USA* 108:20881–20890.
66. Ticozzi N, et al. (2011) Mutational analysis reveals the FUS homolog TAF15 as a candidate gene for familial amyotrophic lateral sclerosis. *Am J Med Genet B Neuropsychiatr Genet* 156B:285–290.
67. Fey EG, Krochmalnic G, Penman S (1986) The nonchromatin substructures of the nucleus: The ribonucleoprotein (RNP)-containing and RNP-depleted matrices analyzed by sequential fractionation and resinless section electron microscopy. *J Cell Biol* 102:1654–1665.
68. Guzzo CM, et al. (2012) RNF4-dependent hybrid SUMO-ubiquitin chains are signals for RAP80 and thereby mediate the recruitment of BRCA1 to sites of DNA damage. *Sci Signal* 5:ra88.
69. Anderson P, Kedersha N (2009) RNA granules: Post-transcriptional and epigenetic modulators of gene expression. *Nat Rev Mol Cell Biol* 10:430–436.
70. Schultz J, Milpetz F, Bork P, Ponting CP (1998) SMART, a simple modular architecture research tool: Identification of signaling domains. *Proc Natl Acad Sci USA* 95: 5857–5864.
71. March ZM, King OD, Shorter J (2016) Prion-like domains as epigenetic regulators, scaffolds for subcellular organization, and drivers of neurodegenerative disease. *Brain Res* 1647:9–18.
72. Dao TP, et al. (2018) Ubiquitin modulates liquid-liquid phase separation of UBQLN2 via disruption of multivalent interactions. *Mol Cell* 69:965–978.e6.
73. Gilks N, et al. (2004) Stress granule assembly is mediated by prion-like aggregation of TIA-1. *Mol Biol Cell* 15:5383–5398.
74. Reineke LC, Dougherty JD, Pierre P, Lloyd RE (2012) Large G3BP-induced granules trigger eIF2$\alpha$ phosphorylation. *Mol Biol Cell* 23:3499–3510.
75. Tourrière H, et al. (2003) The RasGAP-associated endoribonuclease G3BP assembles stress granules. *J Cell Biol* 160:823–831.
76. Sarkar J, Myong S (2018) Single-molecule and ensemble methods to probe initial stages of RNP granule assembly. *Methods Mol Biol* 1814:325–338.
77. Patel A, et al. (2017) ATP as a biological hydrotrope. *Science* 356:753–756.
78. Goulet I, Boisvenue S, Mokas S, Mazroui R, Côté J (2008) TDRD3, a novel Tudor domain-containing protein, localizes to cytoplasmic stress granules. *Hum Mol Genet* 17:3055–3074.
79. Jayabalan AK, et al. (2016) NEDDylation promotes stress granule assembly. *Nat Commun* 7:12125.
80. Adegoke OO, et al. (2017) Overexpression of ubiquilin-1 alleviates Alzheimer's disease-caused cognitive and motor deficits and reduces amyloid-$\beta$ accumulation in mice. *J Alzheimers Dis* 59:575–590.
81. Safren N, Chang L, Dziki KM, Monteiro MJ (2015) Signature changes in ubiquilin expression in the R6/2 mouse model of Huntington's disease. *Brain Res* 1597:37–46.
82. Hanson KA, Kim SH, Wassarman DA, Tibbetts RS (2010) Ubiquilin modifies TDP-43 toxicity in a Drosophila model of amyotrophic lateral sclerosis (ALS). *J Biol Chem* 285:11068–11072.
83. Zhang T, et al. (2018) FUS regulates activity of MicroRNA-mediated gene silencing. *Mol Cell* 69:787–801.e8.
84. Burke KA, Janke AM, Rhine CL, Fawzi NL (2015) Residue-by-residue view of in vitro FUS granules that bind the C-terminal domain of RNA polymerase II. *Mol Cell* 60: 231–241.